Absorption modulation induced by electron beam excitation of strained $In_{0.2}Ga_{0.8}As/GaAs$ multiple quantum wells

D. H. Rich, K. Rammohan, Y. Tang, and H. T. Lin
Photonic Materials and Devices Laboratory, Department of Materials Science and Engineering, University of Southern California, Los Angeles, California 90089-0241

J. Maserjian and F. J. Grunthaner
Center for Space Microelectronics Technology, Jet Propulsion Laboratory, California Institute of Technology, Pasadena, California 91109

A. Larsson
Chalmers University of Technology, Department of Optoelectronics and Electrical Measurements, S-412 96 Göteborg Sweden

S. I. Borenstain
Jerusalem College of Technology, Jerusalem, Israel 91160

(Received 27 January 1993; accepted 2 April 1993)

The effects of excess carrier generation on excitonic absorption phenomena in *nipi*-doped $In_{0.2}Ga_{0.8}As/GaAs$ multiple quantum wells (MQWs) was examined using a novel technique called *electron beam-induced absorption modulation imaging*. The *nipi*-doping induced barrier height is determined by measuring the frequency response of the absorption modulation as a function of temperature and employing a model which is based on thermal excitation of carriers in the limit of Boltzmann statistics. Spatial steps in the absorption modulation which correlate with the positions and orientation of dark line defects imaged in cathodoluminescence are observed. These results indicate the existence of defects in the MQWs which impede the ambipolar diffusive transport of the spatially separated electron-hole plasma.

I. INTRODUCTION

The spatially separated electron-hole plasma that can be generated in periodically doped *nipi* multiple quantum well (MQW) semiconductor structures exhibits large photooptic effects which can be utilized for applications in photonic devices. Because of large enhancements in the excess carrier lifetime, large plasma densities can be created by relatively weak optical excitation to alter the effective *nipi* band gap, MQW excitonic absorption, and refractive index.[1,2] The InGaAs/GaAs MQW system, owing largely to the transparent nature of the GaAs substrate with respect to the MQW interband transition energies, is a leading candidate for the fabrication of spatial light modulators (SLMs) which are the building blocks of high-information throughput optical computing elements and Fourier-plane image processing devices.[3–5] In *nipi*-doped semiconductors, the spatial modulation in the conduction and valence band edges relative to the Fermi level results in a spatial separation of excited electrons and holes. This spatial separation results in long recombination lifetimes and large ambipolar diffusion lengths.[1–4,6] Theoretical calculations together with Shockley–Haynes-type experiments confirm the large enhancement of the ambipolar diffusion constant.[6] Also, large electron densities can be built up in the QWs with low excitation densities; this can enable an externally controlled modulation of the electron-to-heavy hole (e–hh) QW exciton transitions in absorption through screening and band filling effects.[2–4]

The lifetime enhancement and diffusive transport of the plasma is influenced by the presence of defects, impurities, and statistical spread of dopants in the film. In the InGaAs/GaAs MQW system, misfit dislocations will be generated after a certain critical thickness has been reached. Previously, the electronic and structural properties of misfit dislocations in thick $In_{0.2}Ga_{0.8}As/GaAs$ multiple quantum wells (MQWs) were studied using cathodoluminescence (CL) and transmission electron microscopy.[7,8] Based on the quantification of the luminescence intensity associated with [110]-oriented dark line defects (DLDs), the authors proposed that a *Cottrell atmosphere* of nonradiative point defects surrounding dislocations which are solely confined to the GaAs substrate-to-MQW and GaAs capping layer-to-MQW interfaces is responsible for the observed luminescence behavior.[7,8]

We demonstrate in this article, using a novel approach, that the spatially separated electron-hole plasma can be used as a probe to study the electronic and structural properties of defects which can exist in the MQW regions. We have examined the effects of excess carrier generation on excitonic absorption phenomena in *nipi*-doped $In_{0.2}Ga_{0.8}As/GaAs$ multiple quantum wells (MQWs) using a new technique called *electron beam-induced absorption modulation imaging* (EBIA). The influence of defects on the ambipolar diffusive transport and the excess carrier lifetime are examined with EBIA. Conventional optical techniques, utilizing laser sources for excess carrier generation, have previously been used to measure changes in the absorption spectrum induced by excess carriers in *nipi*-doped MQWs.[2–4]

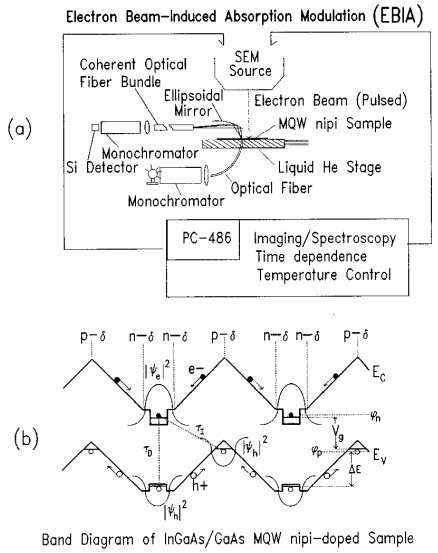

FIG. 1. Schematic of electron beam-induced absorption modulation imaging and cathodoluminescence setup in (a). Band diagram of a MQW *nipi* structure showing spatial separation of electrons and holes which occurs under electron beam excitation (b). The structure is illustrated for the case of δ doping, which results in linear variations in the conduction (E_c) and valence (E_v) band edges relative to the Fermi level. During electron beam excitation, the Fermi-level is split into quasi Fermi levels for electrons and holes (ϕ_n and ϕ_p, respectively). The two distinct intrinsic recombination channels caused by thermally excited spatially direct transitions and spatially indirect tunneling recombination are illustrated with the dotted lines and denoted with lifetimes τ_D and τ_I, respectively.

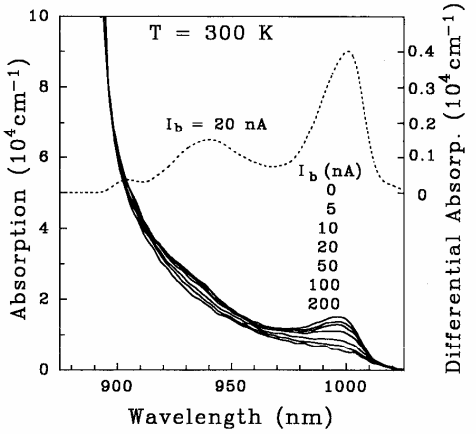

FIG. 2. EBIA spectroscopy measurement of a *nipi*-doped MQW sample for room temperature. The electron beam was focused on a region above the center of the optical fiber, and beam currents are indicated. The electron beam-induced absorption changes are caused by band filling and quenching of the hh–e exciton. Differential EBIA spectroscopy measurements (dashed lines) were obtained by blanking the electron beam source.

II. EXPERIMENT

In EBIA, the excess carriers are generated by a high energy electron beam within a scanning electron microscope (SEM); a JEOL 840-A SEM was used in this work. The electron probe has the advantage that the electron-hole pair density in the excitation volume is nearly homogeneous for appropriate beam energies (i.e., all QW layers can be excited equally).[9,10] By utilizing the scanning capability of the SEM, spatial imaging information, in addition to spectral absorption variations can be obtained. The experimental setup utilizes a modified cathodoluminescence system to collect light which is transmitted through the MQW structure as illustrated in Fig. 1(a). A multimode optical fiber with a 100 μm core diameter is used to transmit light from a tungsten light source dispersed by a monochromator to the backside of the sample in the SEM vacuum chamber. The technique utilizes lock-in detection by chopping either the light source from the monochromator or the electron beam source. The images reveal an absorption modulation contrast caused by the influence of intrinsic and extrinsic recombination channels on the diffusion of spatially separated carriers to the vicinity of the optical fiber. Lifetime effects and recombination centers are examined by varying the sample temperature and by modulating the electron beam source to study the carrier dynamics.

The sample (designated D92) was grown by molecular beam epitaxy, and consists of 44 $In_{0.2}Ga_{0.8}As$ QWs, each 65 Å wide, and separated by 780 Å thick GaAs barriers. In the center of each GaAs barrier a *p*-type Be-doping plane with a sheet density of 9.0×10^{12} cm^{-2} was inserted. On both sides of the QWs, using 100 Å thick spacer layers, *n*-type Si-doping planes with a sheet density of 3.0×10^{12} cm^{-2} were inserted. Using Fermi statistics and charge neutrality conditions, these doping levels give ideally an excess hole concentration and a depletion-induced modulation depth approximately equal to the effective band gap of the InGaAs QWs. The δ doping causes a linear variation in the band edges along the growth direction, as shown in Fig. 1(b). During electron-hole pair generation, electrons will be attracted to the QWs and the holes to the barrier region midway between the wells, resulting in their spatial separation.

III. RESULTS AND DISCUSSION

A. Electron beam-induced modulation of the QW absorption

Absorption spectra for various electron beam currents are shown in Fig. 2, and were obtained by chopping the monochromator probe. The effective QW absorption coefficients were calculated according to $(-L_{\text{eff}})^{-1}\ln T$, where T is the measured normalized transmission through the sample and L_{eff} is the total thickness of the MQW structure. The total light power through the fiber was $\sim10^{-7}$ W with a spectral resolution of 1 nm. Other measurements using various powers confirmed that SEED (self-electro-optic device) effects were negligible. The hh1–e1 exciton peak is located at 996 nm for a sample temperature of 300 K. The peak is seen to quench as the current level is increased; this is a result of the screening of the Coulomb interaction in the QWs by the electron

plasma. The peak absorption at the exciton resonance, α_{max}, is related to the two-dimensional electron density in the QW, δn_e, by the expression

$$\alpha_{max}=\frac{\alpha_0}{1+(\delta n_e/n_{sat})}, \tag{1}$$

where α_0 is the absorption coefficient in the absence of excitation and n_{sat} is the saturation carrier density which was found to be $\sim 1\times 10^{11}$ cm^{-2} from optically induced absorption modulation measurements.[2,11] The differential absorption spectrum (dashed curves of Fig. 2) was obtained by chopping the electron beam, this enables an observation of the higher lying excitonic transitions. At $T=300$ K, the peak located at ~ 940 nm is due to transitions from the valence band continuum edge (hh3) to the first confined electron state e1. The peak located at ~ 905 nm is due to transitions between the second quantized states (hh2–e2) as well as transitions between the valence band continuum and the second quantized electron state (hh3–e2), as these fall close to each other in energy.

The size and shape of the electron-hole pair generation region depends on the beam energy. A maximum generation depth of ~ 6 μm is expected for the 35 keV beam energy used in this study,[9,10] this is sufficient for a near-uniform excitation of the 3.7 μm MQW region of sample D92. The number of electrons per unit area at steady-state conditions, δn_e, deposited in a QW is estimated by[2,9,10]

$$\delta n_e=\tau D\frac{dE_b}{dz}I_b(1-f)\Big/\pi L_A^2 eE_i, \tag{2}$$

where D is the MQW period, dE_b/dz is the electron beam "depth dose" or energy dissipation function, I_b is the beam current density, f is the fractional beam loss due to backscattered electrons (and, for most cases, $f\ll 1$), e is the electric charge, E_i is the valence electron ionization energy (i.e., the energy required to form an electron-hole pair and is about three times the band gap for semiconductors), and L_A is the effective ambipolar diffusion length which will also depend on the excitation conditions. Due to the generation of excess carriers, the effective *nipi* band gap V_g will increase (by reduction of the built-in space charge field) and this results in a decrease in recombination time τ according to the expression[2]

$$\tau=\tau_0 e^{-\beta\delta n_e}, \tag{3}$$

where τ_0 and β are parameters which depend on the temperature and the MQW *nipi* structure. The quenching of the hh1–e1 exciton absorption coefficient at $T=300$ K, in Fig. 2, is seen to depend approximately logarithmically on the beam current as expected from the reduction of the recombination lifetime with increasing carrier density [using Eqs. (1)–(3)].

B. Temperature and temporal dependence of the excess carrier recombination

The recombination of the spatially separated carriers occurs through spatially indirect radiative tunneling recombination and spatially direct recombination of thermally excited carriers, as illustrated by the arrows in Fig. 1(b). The recombination rate τ^{-1} in the simplest model, can be expressed as the sum of the recombination rates for the spatially direct and spatially indirect channels, which are denoted as τ_D^{-1} and τ_I^{-1}, respectively, and is given by

$$\frac{1}{\tau}=\frac{P_I}{P_T}\frac{1}{\tau_I}+\frac{P_D}{P_T}\frac{1}{\tau_D}, \tag{4}$$

where P_I and P_D are the steady-state sheet densities of holes in the regions between the QWs and in the QWs, respectively, and P_T is the sum of P_I and P_D. Since the large modulation depth, causes the hole QW levels to be several kT below the hole quasi-Fermi level under typical excitation conditions,[2–4] we can use Boltzmann statistics to describe the ratio of the populations, i.e., $P_D/P_I\propto e^{-\Delta E/kT}$, where ΔE is an activation energy for excitation of holes at the quasi-Fermi level to the QW hole levels. In the high-temperature limit, where the carrier lifetime is mainly determined by the fraction of holes which occupy states in the valence band QWs through thermal excitation, Eq. (4) simplifies to $\tau\propto e^{\Delta E/kT}$. In order to test this model and further study the dynamics of carrier recombination, we have measured the frequency response of the transmission modulation for various temperatures. The normalized transmission modulation intensity as a function of the frequency of the pulsed electron source (fixed at the fiber center) and fixed electron beam current is plotted for the various temperatures indicated in Fig. 3. The lifetime of the excess carriers was estimated by the measured 3 dB frequency response, i.e., $\tau_{3\ dB}=1/(2\pi f_{3\ dB})$. The values for $\tau_{3\ dB}$ as a function of temperature for the electron beam currents of 0.1, 0.3, 1.0, 3.0, and 10 nA are shown in Fig. 4. For each of the beam current conditions, the data shows that $\log(\tau_{3\ dB})\propto 1/kT$ for temperatures in the range $320\lesssim T\lesssim 220$ K. For lower temperatures the lifetime approaches an asymptotic limit, where spatially indirect tunneling recombination of holes determines mainly the total lifetime. The solid lines running through the points in Fig.

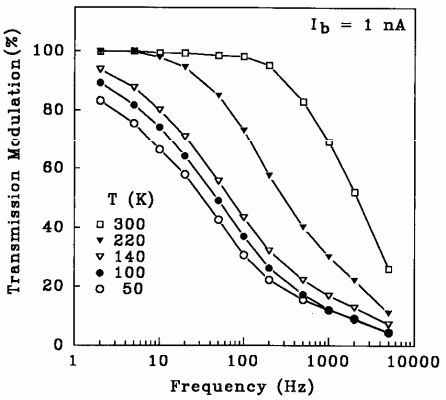

FIG. 3. Normalized transmission modulation as a function of the electron beam blanking frequency. The frequency response was examined for various temperatures which are shown. Changes in response are due to the lifetime dependence on the temperature.

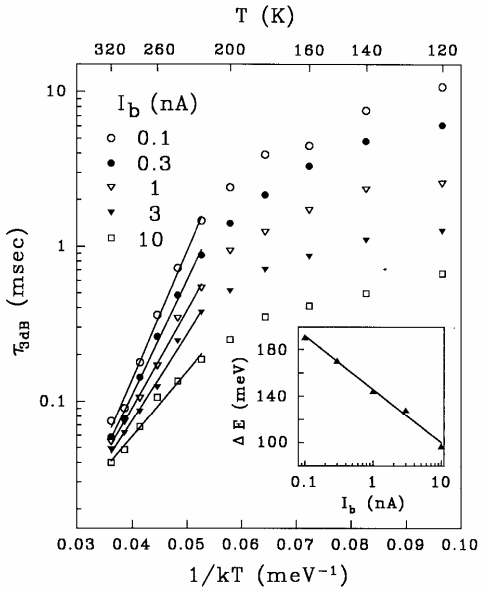

FIG. 4. The measured 3 dB lifetime $\tau_{3\ dB}$ as a function of the temperature for various excitation currents shown. The straight lines shown from $320 \leqslant T \leqslant 220$ K indicate the linear fits of $\log(\tau_{3\ dB})$ vs $1/kT$ which was used to determine the activation energy. The activation energy ΔE as a function of the beam current is shown as an inset.

4 indicate results of linear fits that were used to determine ΔE; the values of the activation energies are plotted as a function of the beam current in the inset of Fig. 4. A logarithmic dependance is evident (i.e., $\Delta E \propto \log I_b$) and a line is schematically shown through the data. The results of Fig. 4 are further consistent with the notion that the effective *nipi* band gap V_g is expected to vary linearly with $\log I_b$. We note that ΔE and τ_I will depend on τ since $\delta V_g = (e/\epsilon)\delta n_e$ (where ϵ is the permittivity), from electrostatic theory and $\delta n_e \propto \log(\tau/\tau_0)$, from Eq. (3). Therefore, a fit of $\tau_{3\ dB}$ to Eq. (4) over a large temperature range, while keeping ΔE and τ_I constant, is not strictly valid. The value of ΔE reflects the position of the hole quasi-Fermi level relative to the QW hole energy levels, and is thus a quantity of fundamental interest in understanding the carrier dynamics in *nipi* MQW structures. For high temperatures $T \gtrsim 220$ K, the recombination is dominated by thermal excitation of the carriers into the QWs, as evidenced from the Arrhenius behavior in Fig. 4. The values of ΔE seen in Fig. 4 for these excitation conditions are much smaller than those expected from the ideal modulation depth of ~ 1200 meV for this structure, based on Fermi statistics and electrostatic theory.[3] In Sec. III C, we will explore defect-related mechanisms which can lower the barrier height.

C. Influence of defects on diffusive transport of carriers

A panchromatic CL image of the sample is shown in Fig. 5(a) with a 115 K temperature. The cathodoluminescence is primarily due to the MQW exciton associated with the e1–hh1 transition.[7,8] The dark line defects (DLDs) are oriented along the $[1\bar{1}0]$ and [110] directions. Based on previous cathodoluminescence and transmission electron microscopy data, Rich and co-workers have proposed that a Cottrell atmosphere of point defects situated between the MQW-to-GaAs interfacial regions are responsible for the DLDs.[7,8] An EBIA image [shown in Fig. 5(b)] was obtained by detecting the transmitted signal at $\lambda = 948$ nm,

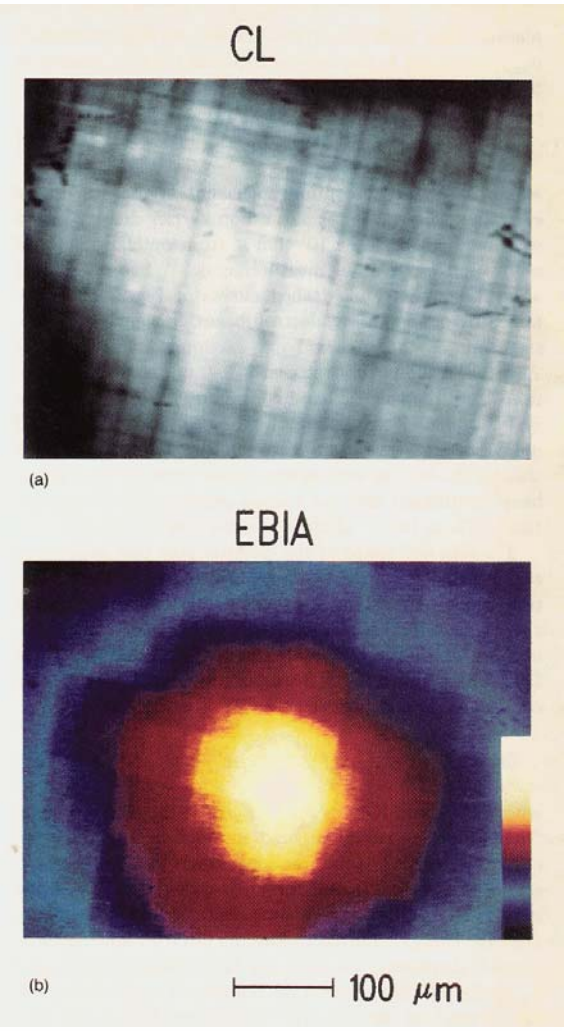

FIG. 5. Cathodoluminescence (CL) image (a) and EBIA image (b) of the same region of a *nipi*-doped MQW structure. The CL image of the e–hh exciton luminescence is represented by a gray scale, where bright regions correspond to an increase in luminescence intensity relative to darker regions. Dark line defects (DLDs) are observed to run along both [110] directions. The EBIA image is displayed using a false-color scale for the absorption modulation intensity. DLDs are seen to correspond with the positions and orientations of absorption modulation steps, which are represented by sharp changes in color along the same high symmetry [110] directions in (b).

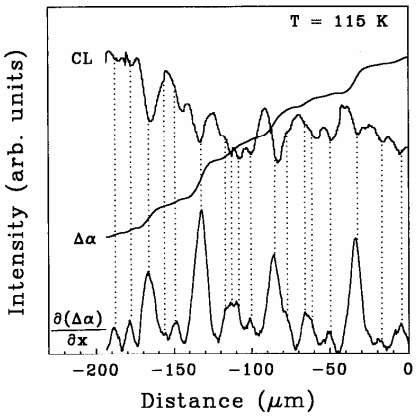

FIG. 6. Histograms (intensity vs position) of cathodoluminescence (CL), absorption modulation ($\Delta\alpha$), and its derivative $\partial\Delta\alpha/\partial x$ as a function of the distance (x) from the center of the optical fiber along [110]. The center of the steps in the absorption modulation (peaks in the derivative) are seen to correlate strongly with the minima and shoulders seen in the CL line scan. The minima in the CL scans correspond to the dark line defects seen in the CL image of Fig. 5(a).

corresponding to the e1–hh1 exciton absorption at $T=115$ K. The electron beam was pulsed at a fixed frequency of 500 Hz while rastered in two-dimensions across the sample to generate a 640×480 pixel image with the differential absorption intensity value stored in one byte of memory per pixel. A conventional gray scale display is inadequate to demonstrate the full information content of the image, due to the monotonic decrease of the modulation intensity as the beam is moved away from the fiber center (white region in the image). The color scale (representing a linear intensity mapping) is shown at the lower right portion of Fig. 5(b). The EBIA image of Fig. 5(b) shows the influence of structural defects on the diffusive transport of carriers with a μm-scale resolution.

These results demonstrate, remarkably, that the orientation and positions of the steps seen in the absorption modulation correspond with the orientation and position of DLDs seen in the CL image. A histogram of the imaging results of Fig. 5 is presented in Fig. 6. The curves illustrate the intensity versus electron beam position relative to the fiber center (distance=0) along [110] for CL, the absorption modulation $\Delta\alpha$, and its derivative $\partial\Delta\alpha/\partial x$. The center of the steps in $\Delta\alpha$ shows up as peaks in the derivative scan. Vertical dotted lines are drawn in the figure to illustrate the strong correlation between dips and shoulders in the CL intensity at DLDs and the positions of the steps observed in the absorption modulation. As the electron beam is positioned away from the fiber center, we would expect a monotonic decrease in the absorption modulation intensity caused by the in-plane diffusion of carriers away from the electron beam excitation region. The transport of electrons and holes is influenced by the presence of point defects which are related to the existence of DLDs seen in the CL image.

The presence of point defects lying in the regions delineated by the DLDs in CL imaging can influence the diffusion process in the following ways: (i) by creating diffusion barriers, (ii) by creating midgap recombination centers, and (iii) by affecting the lifetime of spatially indirect transitions (i.e., τ_I). Point defects can create local variations in the band edges relative to the Fermi level; the depletion length will depend on the charge associated with the defect and the local dopant concentration. Since the electrons and holes in the plasma are confined to the n- and p-type regions, respectively [see Fig. 1(b)], a defect-induced change in the band edges will push the Fermi level (or quasi-Fermi level under excitation) closer to the middle of the gap. In case (i), this band bending will cause the majority carriers to be repelled from the point defects and the Cottrell atmosphere of defects will act as a barrier to diffusion. A large excess carrier concentration will reduce the band bending, in a manner similar to the barrier reduction which occurs in a surface photovoltaic shift. In case (ii), the barrier reduction will result in an attendant increase in overlap between wave functions of the midgap defect states and the majority carriers. A lower average value of ΔE in the vicinity of defects is consistent with the values found in the ΔE measurement of Fig. 4. Also, thermally assisted defect-induced recombination of majority carriers can occur at high temperatures. This is similar to the existence of thermal activation barriers for minority carriers caused by defects in uniformly doped semiconductors which causes the enhancement of nonradiative recombination at high temperatures.[12] In case (iii), a large density of point defects will increase the average value of V_g (reduce ΔE), resulting in a smaller value of τ_I. While the three cases are not exhaustive, they illustrate possible ways in which a Cottrell atmosphere of defects can cause the measured steplike response in the EBIA image of Fig. 5(b).

Recent theoretical calculations by Jonsson *et al.* have shown that the expected lifetime is several orders of magnitude longer than the lifetime measured by an optically induced absorption modulation technique.[13] The primary cause suggested for this lifetime discrepancy was a spatial redistribution of dopants which would lead to an effective decrease in ΔE, and thus an increase in tunneling recombination and spatially direct recombination of thermally excited carriers.[13] The present structure in the EBIA imaging results demonstrate that extrinsic defect related mechanisms can also effect the lifetime and carrier transport.

IV. CONCLUSION

In conclusion, the modulation of MQW exciton absorption has been demonstrated with use of a high energy electron beam to study the carrier recombination dynamics. The *nipi*-doping induced barrier height ΔE which impedes holes from accessing QW levels is determined by measuring the frequency response of the absorption modulation as a function of temperature and employing a model which is based on thermal excitation of carriers in the limit of Boltzmann statistics. The barrier height is found to depend logarithmically on the electron probe current, consistent with the theory. The application of a new technique, *EBIA*,

demonstrates the power and feasibility of using the spatially separated electron-hole plasma as a probe to study the influence of defects on the ambipolar diffusion of carriers. Steps in the absorption modulation which correlate with the positions and orientation of DLDs in cathodoluminescence are observed. These results strongly support a previous hypothesis which held that [110]-oriented DLDs observed in CL imaging were caused by regions of enhanced densities of a Cottrell atmosphere of point defects.

ACKNOWLEDGMENTS

This work was supported by grants from the USC James H. Zumberge Faculty Research and Innovation Fund and the Charles Lee Powell Foundation. Part of the research described in this article was performed by the Center for Space Microelectronics Technology, Jet Propulsion Laboratory, California Institute of Technology, and was jointly sponsored by the Defense Advanced Research Projects Agency, the Strategic Defense Initiative Organization, Innovative Science and Technology Office, and the National Aeronautics and Space Administration, Office of Aeronautics, Exploration, and Technology.

[1]G. H. Döhler, IEEE J. Quantum Electron. **QE-22**, 1682 (1986); J. Vac. Sci. Technol. B **1**, 278 (1983).
[2]J. Maserjian, P. O. Andersson, B. R. Hancock, J. M. Iannelli, S. T. Eng, F. J. Grunthaner, K.-K. Law, P. O. Holtz, R. J. Simes, L. A. Coldren, A. C. Gossard, and J. L. Merz, Appl. Opt. **28**, 4801 (1989).
[3]A. Larsson and J. Maserjian, Appl. Phys. Lett. **58**, 1946 (1991); Opt. Eng. **31**, 1576 (1992).
[4]A. Larsson and J. Maserjian, Appl. Phys. Lett. **59**, 3099 (1991).
[5]N. Streibl, K.-H. Brenner, A. Huang, J. Jahns, J. Jewell, A. W. Lohmann, D. A. B. Miller, M. Murdocca, M. E. Prise, and T. Sizer, Proc. IEEE **77**, 1954 (Dec. 1989).
[6]K. H. Gulden, H. Lin, P. Kiesel, P. Riel, G. H. Döhler, and K. J. Ebeling, Phys. Rev. Lett. **66**, 373 (1991).
[7]D. H. Rich, K. C. Rajkumar, Li Chen, A. Madhukar, T. George, J. Maserjian, F. J. Grunthaner, and A. Larsson, J. Vac. Sci. Technol. B **10**, 1965 (1992).
[8]D. H. Rich, T. George, J. Maserjian, F. J. Grunthaner, and A. Larsson, J. Appl. Phys. **72**, 5834 (1992).
[9]B. G. Yacobi, J. Appl. Phys. **59**, R1 (1986); see, e.g., B. G. Yacobi and D. B. Holt, *Cathodoluminescence Microscopy of Inorganic Solids* (Plenum, New York, 1990).
[10]T. E. Everhart and P. H. Hoff, J. Appl. Phys. **42**, 5837 (1971).
[11]S. H. Park, J. F. Morhange, A. D. Jeffery, R. A. Morgan, A. Chavez-Pirson, H. M. Gibbs, S. W. Koch, N. Peyghambarian, M. Derstine, A. C. Gossard, J. H. English, and W. Weigmann, Appl. Phys. Lett. **52**, 1201 (1988).
[12]See, e.g., J. I. Pankove, *Optical Processes in Semiconductors* (Dover, New York, 1971), pp. 165–166.
[13]B. Jonsson, A. G. Larsson, O. Sjölund, S. Wang, T. Andersson, and J. Maserjian (unpublished).